Renewable and Sustainable Energy Reviews 93 (2018) 631–641

Contents lists available at ScienceDirect

Renewable and Sustainable Energy Reviews

journal homepage: www.elsevier.com/locate/rser

Techno-economic potential of a renewable energy-based microgrid system for a sustainable large-scale residential community in Beijing, China

Li He[a,b,*], Shiyue Zhang[b], Yizhong Chen[a,b], Lixia Ren[c], Jing Li[b]

[a] State Key Laboratory of Hydraulic Engineering Simulation and Safety, Tianjin University, Tianjin 300072, China
[b] School of Renewable Energy, North China Electric Power University, Beijing, 102206, China
[c] Shanxi Institute of Energy, Shanxi, 030600, China

ARTICLE INFO

Keywords:
Renewable energy
Microgrid
Techno-economic potential
Optimization
Sustainable community

ABSTRACT

In this study, the techno-economic potential and optimal configuration are investigated under various renewable energy (RE)-based, stand-alone and grid-connected microgrid scenarios. HOMER software is employed to assess the physical, operating, and economic performance of the system's components, and to obtain the most cost-effective configuration pattern. The outputs obtained from the case study for a residential community in Beijing can help the decision maker identify the optimal adoption of renewable energy sources, electricity generation, and economic benefits. Results show that there is a very high potential for applying a predominantly RE-based microgrid in a residential community in Beijing, which could supply at least 90% of the onsite electricity demand with 47–100% RE sources. In the grid-connected model, the total net present cost (TNPC) of the microgrid system would be, at most, 57% of the obtained electricity less than that completely from the external grids. Results also indicate that it would be more cost-effective when wind power becomes the main energy source and combined with moderately capacity of solar photovoltaic (PV) in the RE hybrid microgrid system. Additionally, a system with moderate size of batteries tends to be more ecologically friendly and cost-effective both in the stand-alone and grid-connected models than a system without batteries.

1. Introduction

In response to the world energy scarcity and environmental pollution, renewable energy (RE) has been expected to play growing importance role in power generation due primarily to their emission free, environmental friendly and inexhaustible nature. Moreover, distributed generation (DG) technologies based on RE can be considered as suitable options for developing countries like China, where the power demands have significantly increased over the past decade [1,2]. Microgrid can integrate the advantages of RE, coordinate the contradiction between the DG and the external power grids, and make full use of the existing DG technologies. It is an autonomous system which is comprised of various DG technologies, energy storage systems, energy conversion devices, flexible loads, protection, and monitoring devices [3,4]. Such a microgrid system can be operated in a grid-connected scenario or in a stand-alone scenario (disconnected from the external grids) [5]. Thus, it is desired to identify the potential of integrating RE, such as solar photovoltaic (PV) and wind power, into stand-alone microgrid and grid-connected microgrids from a long-term perspective.

Maximizing the economic, technological, and environmental benefits has become one of the major concerns for studies on microgrid systems, because 1) the operation modes of microgrids put in huge differences with conventional electric power systems, and 2) the outputs power of RE are greatly influenced by climatic, meteorological, and environmental. Previously, many researchers have widely studied RE-based microgrid systems. For example, Mamaghani et al. [6] aimed at analyzing the application of RE and diesel generators in a stand-alone microgrid system in off-grid villages in Colombia. Such a RE-based microgrid would be the best candidate in rural areas where grids were not available for realizing off-grid electrification. Mazzola et al. [7] performed an optimization design for a stand-alone microgrid system in India and investigated the potential of the use of wood biomass for electricity generation. The obtained results showed that the integration of RE would have a beneficial effect in the economic perspective for the stand-alone microgrid. The introduction of PV panels would allow a cost of energy (COE) reduction by 19% in comparison with those systems based only on diesel generator. Xu et al. [8] compared diverse configuration schemes for stand-alone microgrids for different load types in the Sdakeni (South Africa) rural areas and provided suitability of such schemes and act as a guideline for balancing cost optimization

* Corresponding author.
E-mail address: helix111@tju.edu.cn (L. He).

https://doi.org/10.1016/j.rser.2018.05.053
Received 10 October 2016; Received in revised form 15 March 2018; Accepted 21 May 2018
1364-0321/ © 2018 Elsevier Ltd. All rights reserved.

Nomenclature

P	the power output, kW
$\overline{R}$	the solar irradiance, kW/m^2
d	the PV derating factor, %
Y	the rated capacity, kW
α	the temperature coefficient of power, %/°C
T	the PV cell temperature, °C
U	the wind speed, m/s
H	the height, m
β	the power law exponent
ρ	the air density, kg/m^3
C	the cost, US$
f	the capital recovery factor
i	the number of the annual real interest rate
N	the number of years
E	the energy, kW h

Subscript

T	the current time step
T,STC	the standard test conditions
hub	the hub height of the wind turbine
anem	the wind speed at anemometer height
TAC	the total annualized cost
load	the load served by the microgrid
grid,sales	the energy sold to the grid

Abbreviation

PV	solar photovoltaic
WT	wind turbine
TNPC	the total net present cost
COE	cost of energy
RE	renewable energy
DG	distributed generation
SOC	state of charge
DOD	depth of discharge
CC	cycle charging
LF	load following
SSOM	steady-state operation model

process and design robustness of such systems. Hafez and Bhattacharya [9] focused on optimizing, planning and operating the design of a hybrid RE-based microgrid with the goal of minimizing the life-cycle cost. Results exposed that the renewable and diesel mixed microgrid would have the lowest life-cycle cost and a fairly small carbon footprint. Akinyele and Rayudu [10] aimed at analyzing techno-economic potential and environmental impact of a PV microgrid for remote communities. This research is conductive to conceptualizing and planning PV microgrids in developing countries. Bekele and Palm [11] investigated the possibility of supplying electricity from a solar–wind hybrid system to an off-grid community, and the sensitivity analysis are carried out. Goodbody et al. [12] gave a feasibility analysis to investigate the available RE options using Hybrid Optimization Model for Electric Renewables (HOMER) software. The results indicated that Ireland would have significant potential for wind energy and hydropower generation. Soshinskaya et al. [13] explored the techno-economic potential for a hybrid RE-based microgrid serving an industrial sized drink water plant in the Netherlands. The results showed a high potential for wind power and solar PV at the site, and the plant can become 70–96% self-sufficient with renewable electricity.

Since most of these studies are mainly concentrated on the small-scale off-grid area, it is usually easy to get into trouble when grid-connected scenarios with larger load are considered. Therefore, it is necessary to investigate the feasibility of predominantly RE-based microgrids at such energy intensive power demand of an area such as Beijing. However, it is usually easy to get into trouble when a comprehensive work needs to be conducted on techno-economic evaluation and configuration of a microgrid system. Use the capacity shortage to assess the system technological reliability performance, use the life-cycle cost to assess the economic benefit and use the renewable fraction of load to assess the environmental performance for a microgrid system. Besides, there has been little effort taken on both stand-alone and grid-connected microgrid scenarios, especially with the concerns of various RE technologies and actual inputs on their physical, operating, and economic characteristics.

Therefore, this study focuses on seeking the optimal integration of available RE and conventional fossil energy to supply electrical demand in a reliable manner and good economic benefit to the residential community. Both grid-connected and stand-alone microgrid scenarios were considered. On one hand, the power system's physical behaviors were modeled to apply the technical analysis. On the other hand, the life-cycle cost for installing and operating the system over its lifetime is used to be the main optimization objective to assess different designs of the microgrid system. The rest of the paper is organized as follows: In Section 2, a residential community with a large residential electricity load in Beijing is taken as a specific example to establish the economic model of the microgrid system and the steady-state operation model (SSOM) of the components. The load data and energy source information used in the study also described in this section. Section 3 presents the main results of the study. Section 4 draws general conclusion.

2. Methodology

To optimize the design of microgrid systems with large residential electricity loads. The purpose of this chapter is to: (1) establish a SSOM and economic model for each component of the microgrid system, with the objective of minimizing the life-cycle cost; (2) Use this model to deal with a real case – located in a residential community in Fang Shan

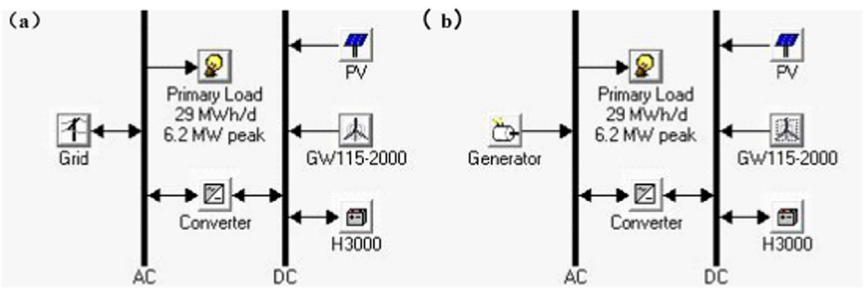

Fig. 1. The grid-connected (a) and off-grid power (b) systems model.

District, Beijing, China, located at 39.70° latitude, 115.96° longitude; (3) formulate indicators for technical-economic assessment of optimized configuration options.

Many factors, e.g., the diversity of the configuration schemes, RE electricity output, load demand and the uncertainty of key parameters (such as fuel prices), may result in the difficulty and complexity of the system during the simulation, optimization, and sensitivity analysis processes [14,15]. HOMER power system simulation software, developed by the National Renewable Energy Laboratory of the United States, is used to perform the processes as required by this study due to its public availability for microgrids modeling, and its ease of implementation [16].

The possible components in the hybrid microgrid system consist of wind turbine (WT), PV, battery, fossil-based generation (either through a local generator or a power grid) and AC/DC converter. Fig. 1 shows the grid-connected (a) and stand-alone (b) systems.

2.1. Electrical load

One of the most important steps in this type of studies is power demand analysis of end users and proposing an electrical load model as real as possible. Assume that the electrical load of the large residential community may not change much in recent years and a 10 GW h annual electricity demand is used in this model. The average daily power consumption is about 28,634 kW h; the peak load is about 6169 kW. The annual electricity consumption curve, as well as the weekday and weekend load curves, is shown in Fig. 2.

As seen from Fig. 2, there are higher power demands during the winter and summer seasons than others, mainly arising from the need of heating in winter and air-conditioning in summer. The daily electrical loads also follow the oscillating distribution, with higher power demand being during the daytime and less at night and the peak load concentrating upon 17:00–21:00. Besides, there is higher power consumption during weekends than working days.

To make the load data more realistic, the data is synthesized by specifying typical daily load profiles and then adding randomness. So, a random variability of 20% day-to-day and 15% time-step-to-time-step would be adopted in the study.

2.2. Major system components

The available RE sources that can provide electricity are wind and solar sources. The following sub-sections give the details of these two RE sources and the SSOM of the main components in the microgrid system, including PV, WT, storage, and fossil-based generation.

2.2.1. Solar photovoltaic

The daily radiation and clearness index of the residential community in Beijing were obtained from the U.S. National Solar Radiation Database with 40 km × 40 km cell dimensions. The annual solar horizontal radiation is shown in Fig. 3, with the average daily one being 4.12 kW h/m^2.

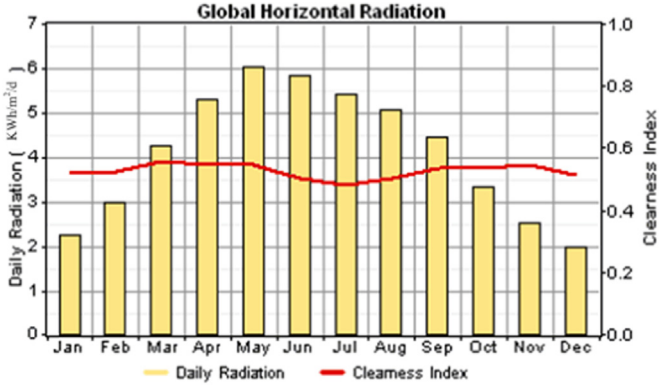

Fig. 3. Annual solar horizontal radiation.

The PV module chosen for this study was monocrystalline silicon cell TSM-175D, which was manufactured by Trina Solar. The final power produced by solar PV was influenced by many factors [17–20], i.e. (1) solar irradiance, (2) characteristics of the PV cells (e.g., conversion efficiency, placement of the PV panels and derating factor) (Table 1), and (3) the PV cells temperature (Table 2).

The temperature coefficient of power normally has a negative impact, meaning that the efficiency of the PV array would decrease with the increase in cell temperature [21]. The average monthly ambient temperature data obtained from China meteorological data network were used in the model. The advanced solar PV properties of considering the effect of temperature are shown in Table 2.

The equation used to calculate the output of the PV array is shown as follows [22]:

$$P_{PV} = \frac{\overline{R}_T}{\overline{R}_{T,STC}}[d_{PV}\, Y_{PV}(1 + \alpha_{PV}(T_C - T_{C,STC}))] \quad (1)$$

where: $\overline{R}_T$ is the solar radiation incident on the PV array of the site [kW/m^2]; $\overline{R}_{T,STC}$ is the solar irradiance at STC[1 kW/m^2]; d_{PV} is the PV derating factor [%]; Y_{PV} is the rated capacity of the PV array [kW]; α_{PV} is the temperature coefficient of power [0.44%/°C for the chosen PV module]; T_C is the PV cell temperature [°C]; $T_{C,STC}$ is the PV cell temperature at STC [25 °C].

Assume the equivalent hours for annual full solar load and the annual electricity demand for the residential community to be about 1500 h [23,24] and 10 GW h, respectively, then the largest capacity configuration of PV modules would be around 6900 kW to meet the

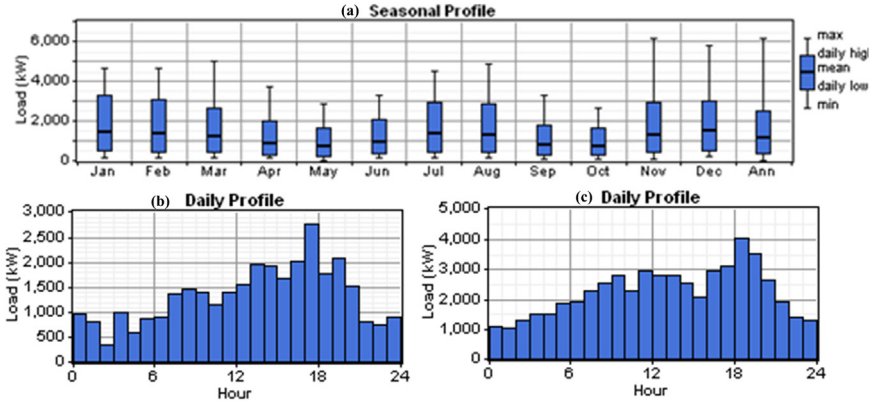

Fig. 2. The electricity consumption curves, where (a), (b), and (c) represent the annual load profile, a weekday in January load profile, and a weekend in January load profile, respectively.

Table 1
Solar PV properties.

Variable	Description	Value
Derating factor	The factor was applied to calculate the reduced power output in real-world operating conditions compared to the rated conditions.	80%
Slope (degrees)	In the fixed-slope system, the panels are mounted with inclination angles that are roughly equal to the latitude of the site, which can obtain the maximize energy production.	39.716
Azimuth (degrees)	The direction towards which the PV panels face. In the fixed-azimuth system, the panels are always installed towards the equator. Beijing is in the northern hemisphere, thus 0 ° azimuth is used in this model.	0
Ground reflectance	The fraction of solar radiation incident on the ground would be reflected by the ground. A typical value (i.e., 20%) in grass-covered areas is adopted in this model.	20%

demand. In order to see the effects of the PV systems size on obtaining optimal configuration, five solar PV system sizes (0, 1.7 MWp, 3.4 MWp, 5.2 MWp and 6.9 MWp) are considered.

2.2.2. Power converter

A converter was incorporated into the microgrid system where the DC components were used to serve as the AC loads or vice-versa. A converter can be an inverter (converts DC electricity to AC electricity), rectifier (converts AC electricity to DC electricity), or both [25]. The SG100k3 inverter was adopted. The efficiency of the inverter and rectifier were assumed to be 90% and 85%, respectively. Assume that the inverter can operate simultaneously with an AC generator and the rated capacity of the rectifier relative to that of the inverter is 100%.

2.2.3. Wind turbine

The wind power mainly depends on the wind speeds at the specific location [26]. The wind data used in this model were obtained from the China Meteorological Data Network. The average annual wind speed was about 4.53 m/s, which was measured at an anemometer height of 10 m. The average monthly measured wind speed is shown in Fig. 4.

GW115-2000 kW WT was selected, which was manufactured by Goldwind Science & Technology. This manufacturer has become the biggest WT maker in the world in 2015. Besides, GW115-2000 kW type is suitable for the local environment of low or medium wind speed and higher turbulence intensity. The WT characteristics data were obtained from the Goldwind website [27], with the power curve being shown in Fig. 5.

In order to adjust the wind speed from an anemometer height to a hub one (i.e., 80 m of the selected turbine), the following equation is used [28]:

$$U_{hub} = U_{anem}\left(\frac{H_{hub}}{H_{anem}}\right)\beta \tag{2}$$

where: U_{hub} is the wind speed at hub height of the WT [m/s]; U_{anem} is the wind speed at anemometer height [m/s]; H_{hub} is the hub height of the WT [m]; H_{anem} is the anemometer height [m]; β is the power law exponent.

The power law exponent was assumed to be 0.19 in the area, by adjusting the wind speeds at hub height of the WT (80 m) leads to an average wind speed of 6.72 m/s. Besides, the altitude (the elevation above mean sea level) affects the air density, leading to affect the WT power output [29]. Therefore, a 200 m average altitude was determined in this model. The WT power output equation applying density

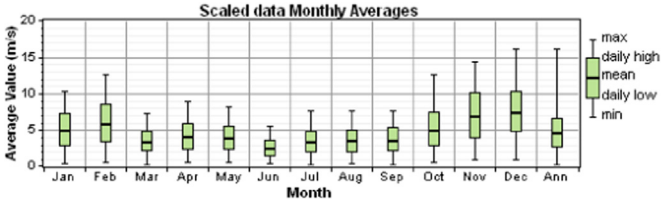

Fig. 4. Average monthly wind speeds at the height of 10 m.

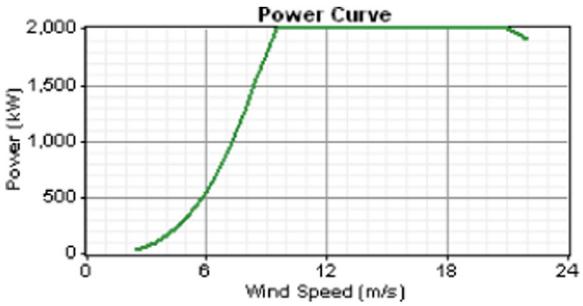

Fig. 5. The GW115-2000 power curve.

correction is used in this model [30]:

$$P_{WT} = \left(\frac{\rho}{\rho_0}\right)\cdot P_{WT,STP} \tag{3}$$

where: P_{WT} is the WT power output [kW]; $P_{WT,STP}$ is the WT power output at standard temperature and pressure [kW];ρis the actual air density calculated based on onsite altitude [kg/m^3];ρ_0 is the air density at standard temperature and pressure [kg/m^3].

2.2.4. Storage and fossil-based generation

Because RE has intermittent characteristics, a RE-based microgrid requires electricity storage equipment, fossil-based generation or their both in order to ensure a constant power supply, especially in a stand-alone scenario [31,32]. Hoppecke3000 [33] batteries were adopted in this model. The chosen battery has a nominal voltage of 2 V and nominal capacity of 3000 Ah. The chosen battery's minimum state of charge (SOC) is 30%, and the round trip DC-to-storage-to-DC efficiency of the battery bank is assumed to have a constant efficiency of 86%. The lifetime curve of the chosen battery is shown as Fig. 6.

Table 2
Advanced solar PV properties considering the effects of temperature.

Variable	Description	Value
Temperature coefficient of power for the chosen PV module	A number indicating how strongly the power output of the PV array depends on cell temperature.	− 0.44%/°C
Nominal operating cell temperature for the chosen PV module	The surface temperature that the PV array would reach if it were exposed to 0.8 kW/m^2 of solar radiation, an ambient temperature of 20 °C, and a wind speed of 1 m/s.	45°
Efficiency at standard test conditions for the chosen PV module	The maximum power point efficiency under standard test conditions (STC) (i.e., a radiation of 1 kW/m^2, a cell temperature of 25 °C, and no wind).	15.9%

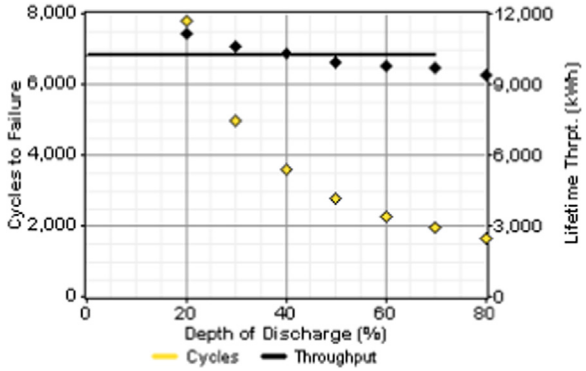

Fig. 6. The battery lifetime curve.

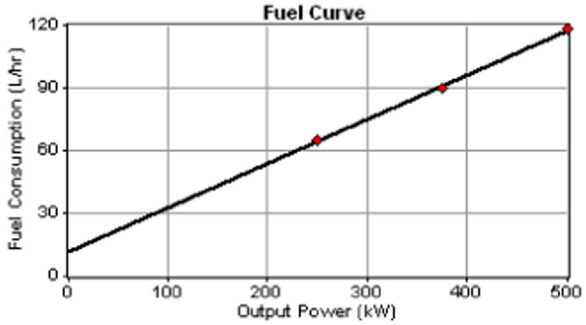

Fig. 7. The fuel consumption curve.

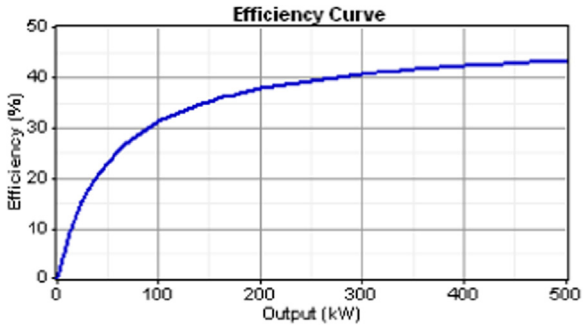

Fig. 8. The generator efficiency curve.

Table 3
Components cost (unit: dollar).

Options	Product model	Initial investment costs	Replacement costs	Annual O &M
Wind	GW115-2000 kW	$1510113 per turbine	$1203007 per turbine	$2010
Solar	TSM-175D	$1066/kW	$902/kW	$30
Converter	SG100k3	$166/kW	$110/kW	$4
Battery	H3000	$722 per battery	$722 per battery	$180
Diesel generator	Cummins KT38-G	$85000	$85000	$98

Fig. 6 shows that the number of cycles to failure declines dramatically with increasing depth of discharge (DOD). The lifetime throughput curve indicates that there is a much weaker dependence on the DOD. Therefore, a simplifying assumption (i.e., the lifetime throughput is not dependent on the DOD) is given by HOMER, meaning that the battery bank lifetime can be estimated simply by observing the amount of energy cycling through the battery bank and no longer considering the depth of the charge–discharge cycles [14,34]. The specified value of lifetime throughput is 10,196 kW h just as the horizontal black line show.

Table 4
Summary of component sizing and life time inputs.

Options	Options on size and unit number	Life time
Wind	0,1,2,3,4,5 turbines	15 y
Solar	0, 1.7 MWp, 3.4 MWp, 5.4 MWp and 6.9 MWp.	20 y
Battery	0400,800,1200,1600,2000,2200.	< 20 y
Converter	1684 kW up to 5894 kW	10,196 kW h
Diesel generator	0 kW,500 kW,1000 kW	15,000 h

Diesel generators are usually applied to improve the system reliability, especially when the system is operated in a stand-alone mode for a long time. The chosen diesel generator is manufactured by Cummins and has 500 kW rated power. Under such a condition (i.e., the minimum generator load ratio is assumed as 30%), the generator cannot be prevented from shutting off but operating at a too low load [35]. Fig. 7 illustrates the fuel consumption curve, with 0.023 L/h/kW fuel curve intercept coefficient and 0.212 L/h/kW fuel curve slope. The generator efficiency curve is shown in Fig. 8.

2.3. Indicators for assessment

2.3.1. Economic analysis

Use life-cycle cost as the optimization goal and evaluate the economic performance of the microgrid system. For evaluating the economic benefits, not only the system's operating costs but also the initial investment and replacement costs should be considered. The life-cycle cost includes all the costs that occur within the lifespan of the system [36,37]. In HOMER model, the total net present cost (TNPC) was chosen to represent the life-cycle cost of the system [38]. In the optimization process, the TNPC was used to rank all the scenarios with different configurations and find out the minimum one. The TNPC was obtained through subtracting the present value of all the revenue from the present value of all the costs incurring over its lifetime. The cost includes the sum of initial capital, replacement, operating and maintenance, fuel, electricity purchasing and pollutant emissions penalties. The revenues include salvage value at the end of the project lifetime and income from selling power to the grid [39]. To calculate the TNPC, the following equation can be used [40]:

$$C_{TNPC} = \frac{C_{TAC}}{f} \tag{4}$$

where: C_{TAC} is the total annualized cost; f is the capital recovery factor, given by the equation [41]:

$$f = \frac{i(1+i)^N}{(1+i)^N - 1} \tag{5}$$

where: N and i are the number of years and the annual real interest rate (the discount rate), respectively. The following equation is used to calculate the levelized COE [42]:

$$COE = \frac{C_{TAC}}{E_{load} + E_{grid,sales}} \tag{6}$$

where: E_{load} is the annualized load served by the microgrid [kW h/y]; $E_{grid,sales}$ is the energy sold to the grid per year [kW h/y]. Table 3 summarizes the cost assumptions for different system components. The replacement cost is assumed to be 90% of the current price. The current diesel price, taken from World Bank data, is 1.1$/liter in China. In the grid-connected mode, the price of buying electricity from the external grids was determined to be 0.08 $/kW h. Table 4 lists the sizes to consider and life time of the components based on the system load demand.

Table 5
Categorized system design for stand-alone models ordered by TNPC.

Number	PV (kW)	GW2.0	Gen (kW)	H3000	TNPC ($)	COE ($/kWh)	Renewable fraction	Capacity shortage	Diesel (L)	Gen (h)
Case 1	1725	4	500	400	16,806,238	0.133	0.91	0.10	224,121	2574
Case 2	0	3	1000	400	17,748,332	0.139	0.76	0.08	570,603	3118
Case 3	3450	4	0	1200	18,441,526	0.147	1.00	0.10	0	0
Case 4	0	5	1000	0	20,100,704	0.157	0.79	0.09	544,440	4141
Case 5	1725	3	1000	0	20,256,648	0.158	0.76	0.09	615,113	4918
Case 6	6900	0	1000	2200	36,408,520	0.292	0.58	0.09	972,962	4776

Table 6
Categorized system design for grid-connected models ordered by TNPC.

Number	PV (kW)	GW2.0	H3000	Grid (kW)	TNPC ($)	COE ($/kWh)	Renewable fraction	Capacity Shortage
Case 7	0	2	400	1000	9034,966	0.055	0.76	0.09
Case 8	1725	1	400	1000	10,165,525	0.070	0.68	0.09
Case 9	1725	3	0	1000	10,984,519	0.060	0.88	0.09
Case 10	0	5	0	1000	12,065,893	0.064	0.89	0.10
Case 11	5175	0	1200	1000	18,459,566	0.137	0.47	0.10

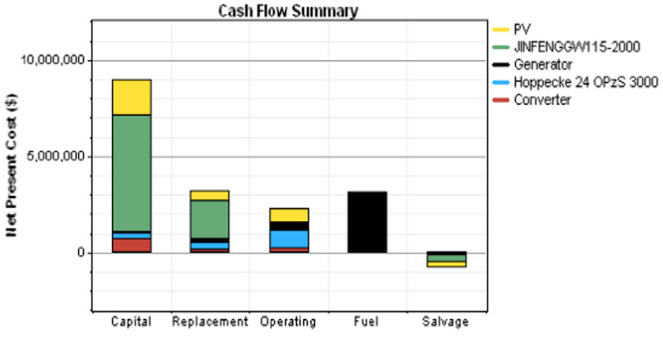

Fig. 9. Cost components for the stand-alone microgrid.

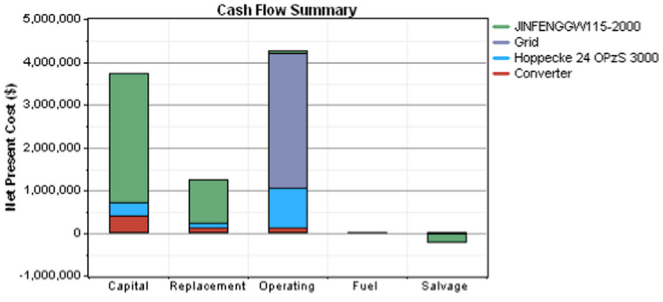

Fig. 10. Cost components for the grid-connected microgrid.

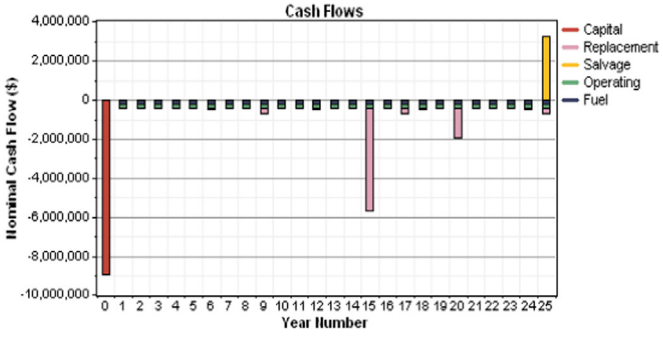

Fig. 11. Annals chronological cash flows for the stand-alone microgrid.

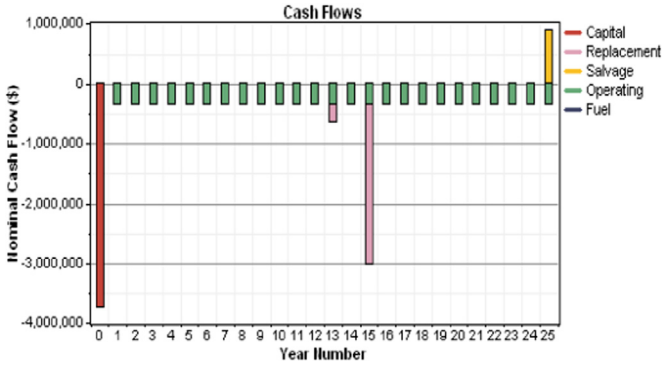

Fig. 12. Annals chronological cash flows for the grid-connected microgrid.

2.3.2. Technological reliability analysis

The capacity shortage is used to assess the system technological reliability performance. The capacity shortage fraction is equal to the total capacity shortage divided by the total electrical demand, its value range between 0 ~ 1, and the smaller the value, the higher the reliability of the microgrid system. Assume that a residential electricity load allows some capacity shortage, which means a shortfall that occurs between the required operating capacity and the actual operating capacity provided by the microgrid system can be accepted. Then, the maximum of 10% of the annual capacity shortage was adopted in this model. To calculate the capacity shortage, the following equation can be used:

$$F_{CS} = \frac{E_{CS}}{E_{demand}} \leq 10\% \tag{7}$$

where: $E_{CS}$is the total capacity shortage [kW h/y], $E_{demand}$is the total electrical demand [kW h/y].

2.3.3. Environmental analysis

The renewable fraction is used to assess the system environmental performance in this study. The air pollutant emissions mainly come from two kinds of microgrid components, respectively for the diesel generator and the external grids. The RE penetration is the fraction of the energy delivered to the load that originated from renewable power sources, which can be calculated as follows [43,44]:

$$F_{ren} = 1 - \frac{(E_{nonren} - E_{gs}) + H_{nonren}}{E_{ser} + H_{ser}} \tag{8}$$

where: $E_{nonren}$is the nonrenewable electrical production [kW h/y],

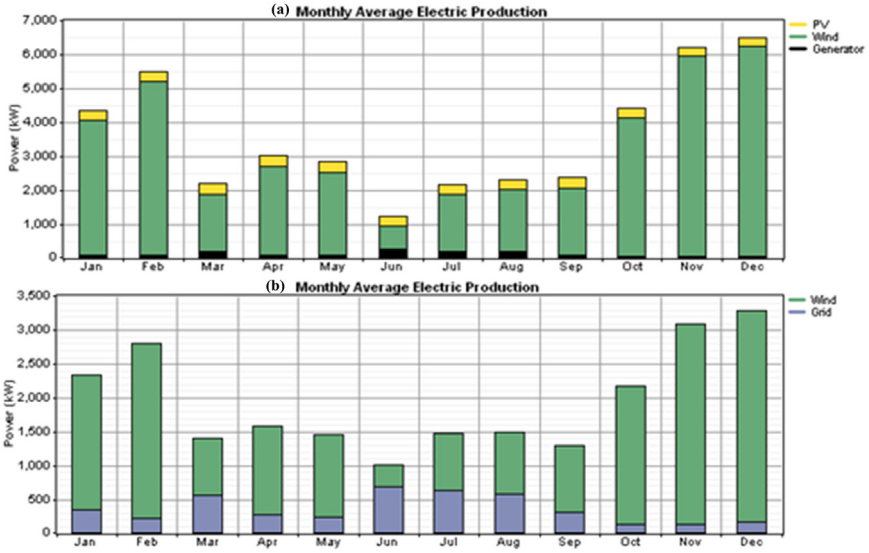

Fig. 13. Monthly average power production in (a) the stand-alone and (b) grid-connected microgrid.

Table 7
Comparison of production and consumption.

Component	Production		Quantity	Value	Load	Consumption	
	Value (kWh/y)	Fraction				Value (kWh/y)	Fraction
The stand-alone system							
PV array	2,549,676	8%	Excess electricity	20,373,960 kWh/y	AC primary load	9,870,418	100%
Wind turbines	27,850,946	89%	Unmet load	580,988 kWh/y	Total	9,870,418	100%
Generator	917,554	3%	Capacity shortage	1,055,512 kWh/y			
Total	31,318,176	100%	Renewable fraction	0.907			
The grid-connected system							
Wind turbines	13,925,473	82%	Excess electricity	3,025,858 kWh/y	AC primary load	9,887,184	77%
Grid purchases	3,089,032	18%	Unmet load	564,228 kWh/y	Grid sales	2,953,057	23%
Total	17,014,504	100%	Capacity shortage	953,634 kWh/y	Total	12,840,241	100%
			Renewable fraction	0.759			

H_{nonren} is the nonrenewable thermal production [kW h/y], E_{gs} is the energy sold to the grid [kW h/y], E_{ser} is total electrical load served [kW h/y], H_{ser} is the total thermal load served [kW h/y].

2.4. Simulation settings

The project lifetime was determined to be 25 years. The annual real interest rate (real interest rate) was assumed to be 6%, which is used to calculate the discount factors and annualized costs from the net present costs [45,46].

In HOMER, there are two major dispatch strategies used to govern the operation of the generator and the battery bank whenever there is not enough RE to supply the load: cycle charging (CC) and load following (LF). Under the load-following strategy, whenever a generator operates, only enough power to serve the load can be produced and the battery bank does not be charged. Under the cycle-charging strategy, a generator will run at as large as possible of its capacity, and the excess generated power will be used to charge the battery bank [47]. The strategy adopted in this study is CC. The set-point SOC was assumed to be 80% in this model, which means that it will keep the system charging the battery bank until the battery bank reaches the set-point SOC. The set-point of SOC tends to avoid the battery bank in low SOC condition for a long time and reduce the battery charge-discharge cycles, thus it will be helpful to extend battery lifetime [48,49].

3. Results and discussions

Microgrids with different configurations were modeled by HOMER to obtain the feasible and the most cost-effective strategy, using the component sizing inputs as shown in Table 4. Table 5 lists the categorized optimization results based on different configurations for the stand-alone system. Table 6 provides the results for grid-connected microgrid system. All the results were ordered by a decreased value of TNPC.

The most optimal strategies with minimum TNPC between the stand-alone and grid-connected microgrid system were then compared and analyzed. The cash flows of the stand-alone and grid-connected microgrid systems are shown in Figs. 9 and 10, respectively. In the stand-alone microgrid system, the cost characteristics of RE power generation and traditional diesel generator are quite different, with the RE power generations being high initial capital costs and low operating costs, while diesel generator tend to be opposite. The TNPC in the stand-alone system is much higher than that in the grid-connected system caused by the large capital cost (i.e., large capacity of WTs and solar PV) and great proportion of fuel cost. While in the grid-connected microgrid system, the operation cost is high due to the purchase of extra power from the external grids.

Figs. 11 and 12 present the annals chronological cash flows of the stand-alone and grid-connected microgrid systems, respectively. The capital cost is larger in the first year because the system needs to install all components at the beginning of the project. The replacement cost would occur when equipment needs to be replaced by the end of their

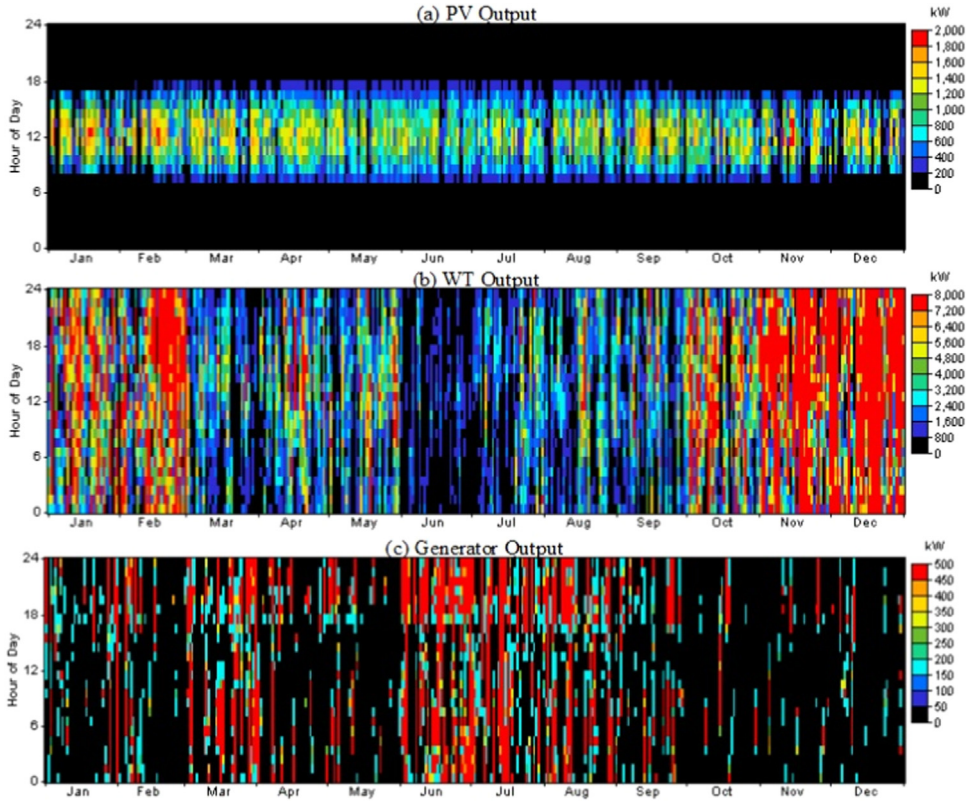

Fig. 14. The (a) solar PV, (b) wind turbine and (c) generator power output.

Table 8
The value of PV, WT and generator power output.

Quantity	PV		WT		Gen	
	Value	Units	Value	Units	Value	Units
Mean output	291	kW	3179	kW	356	kW
Capacity factor	16.9	%	39.7	%	20.9	%
Total production	2,549,676	kWh/y	27,850,946	kWh/y	917,554	kWh/y
Minimum output	0	kW	0	kW	150	kW
Maximum output	1962	kW	7571	kW	500	kW
Hours of operation	4386	h/y	8276	h/y	2574	h/y

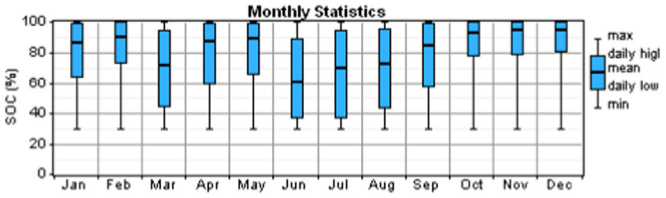

Fig. 15. The relative state of charge.

lifetime. As shown in Fig. 11, the replacement cost of WTs, PV modules and batteries would occur in the fifteenth year, the twentieth year and the eighth year (Table 3), respectively. Additionally, the stable cost for fuel consumption and system operation can exist in the stand-alone microgrid system. The grid-connected system has similar cash-flow property to the stand-alone microgrid one, except that 1) the cost for purchasing fuels was replaced by that for extra power from the external grids, and 2) the replacement cost of batteries would be extended to the thirteenth years.

Comparisons of electrical parameters between the two microgrid scenarios are presented in Fig. 13 and Table 7. As shown in Table 7, the total electricity production under the stand-alone case is much higher than that under the grid-connected case, especially when the capacity shortage of these two cases is almost equal. The renewable energy is intermittent and unable to dispatch, thus, it tends to be a large amount of excess electricity in the predominantly RE-based microgrid. Nearly 20.37 GW h of excess electricity per year can be generated in the stand-alone system, which is approximately 85% higher as than the grid-connected system, where about 3.03 GW h of excess electricity per year can be found. Although a large amount of excess electricity exists in the stand-alone system, such a microgrid can hardly meet the demand of onsite electrical load, especially when the RE sources are insufficient and diesel generator should be relied on. Similarly, the grid-connected microgrid depends on drawing power from the external grids for serving the onsite to against insufficient RE sources.

In the stand-alone case with minimum TNPC, for example, the monthly solar PV, WT and generator power outputs are shown in Fig. 14, and the related parameters of this figure are shown in Table 8. The mean electrical power output of the PV array is 291 kW over the year and the PV penetration of the system (the mean PV power output divided by the mean electrical load) is 24.4%. The operation hours in summer are longer than that in winter. Moreover, the maximum power of the PV array over the year distributes from 11:00–14:00 during a day, while the minimum power (i.e. 0 kW) occurs at night to the next day morning (from around 19:00 to the next day 5:00).

In terms of WTs, their mean power output over the year is 3179 kW with 266% of wind penetration, indicating that a large amount of power output cannot be fully utilized. The stark difference during seasons is that a higher wind speed during the winter months leads to a greater production compared with summer months. Fig. 14(c) shows the generator power output, which indicates that the power outputs between the WT and generator are almost complementary.

The monthly relative state of charge (SOC) for case 1 is shown in Fig. 15. The SOC is the ratio of the current absolute SOC to the

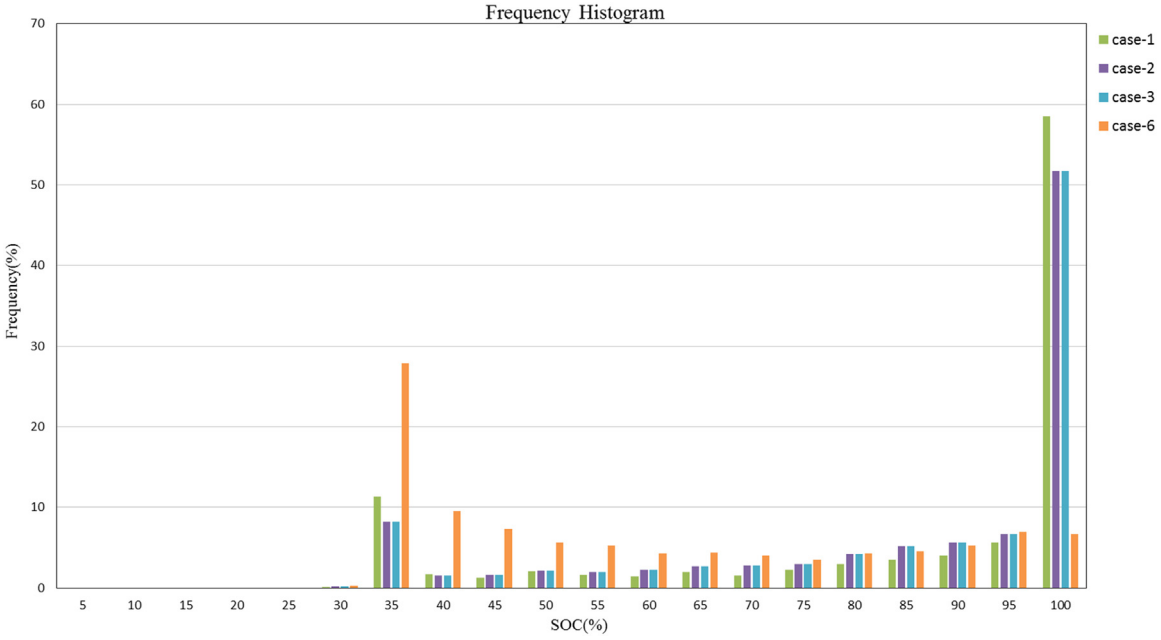

Fig. 16. Battery SOC frequency histogram.

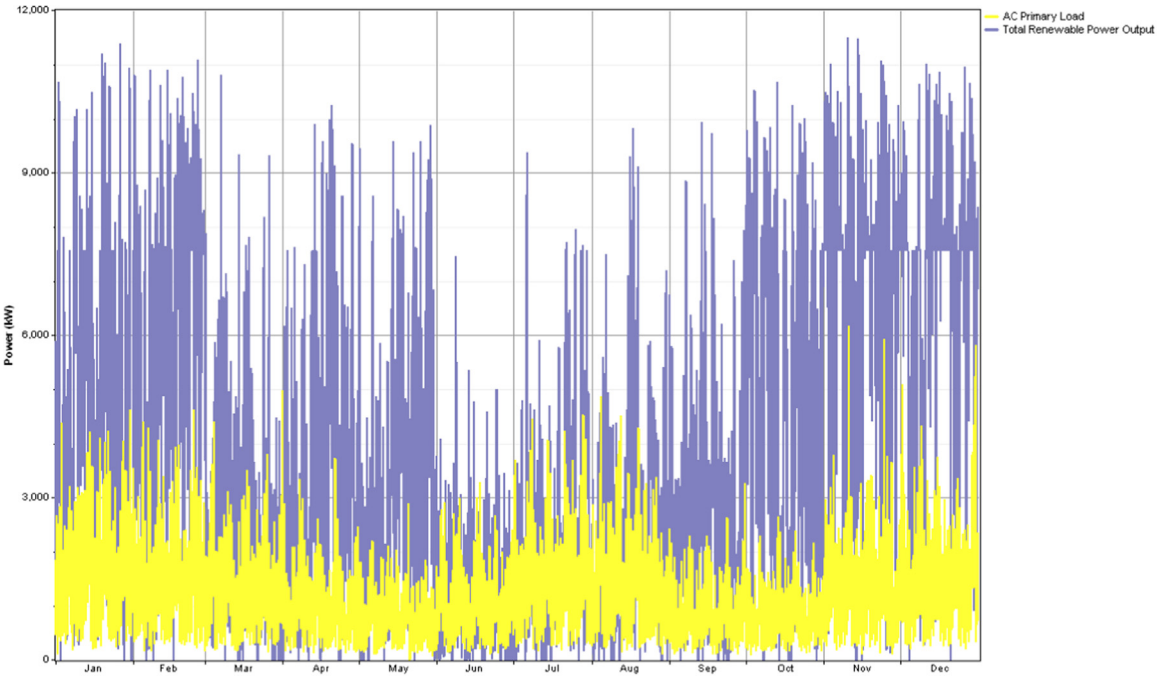

Fig. 17. Monthly electricity load and total renewable power output.

maximum capacity of the battery bank, which means that the SOC is 100% when the batteries are fully charged. In June and July, the daily minimum SOC nearly reach the minimum SOC (i.e., 30%) of the H3000 type. Therefore, the capacity utilization during these two months is higher than the other months due to the higher potential of solar energy and lower wind energy. On the contrary, the mean SOC values are higher in November and December, i.e., the capacity utilization during these two months being lower.

Fig. 16 shows the SOC frequency histogram compared with four cases, i.e., cases 1, 2, 3, and 6. The SOC probability distribution between cases 1, 2, and 3 are almost similar, while case 6 tends to have high fraction of deeper DOD (i.e., low SOC). It is found that the SOC values above 60% in cases 1, 2 and 3 have frequencies of about 82%, 84% and 84%, respectively. In case 6, the frequency of SOC value above 60% is about 44%, which is almost half of that in cases1, 2, and 3. The battery lifetime would decrease with increasing DOD (this has been discussed in Section 2). The battery expected lifetime of case 6 is shorter than the others, which leads to more replacement cost during the project lifetime, thus the economic benefit of case 6 is determined to be the worst one among all the cases.

In the stand-alone microgrid system, a configuration of 100% onsite power demand supplied by RE (3450 kW solar PV and 4 WTs) with 1200 batteries can supply 90% of the onsite electricity demand. Fig. 17 shows the monthly electricity load and total renewable power output of this configuration. The total renewable power output is greater than the electricity load in most of the time. The 4 WTs and 3450 kW solar PV

can make electricity production of 27.85 GW h/y and 5.10 GW h/y, respectively. The total 32.95 GW h annual electricity production is nearly 68% more than the 10.45 GW h annual power demand. Besides, adding either storage or backup generation or both of them can meet the demand in some periods when RE is insufficient or the onsite electricity demand is high. Therefore, it is possible to design a microgrid system with high RE fraction.

It can be obtained that a wind-PV-diesel-battery system combination is the most cost-effective design in the stand-alone cases from the TNPC perspective, which has a high fraction of wind power (4 WTs) and moderate fraction of solar power (1725 kW) combined with 400 batteries and fossil energy. It is also an environmentally friendly combination, since the pollutant emissions are directly related to fuel consumptions, among which the diesel consumption in this combination is up to 41% of the other ones with diesel generator. If a power system without WTs has greater capacity of both solar PV and battery bank (solar PV capacity increase to 4 times and battery bank increase to 5.5 times), the system would has a maximum TNPC of 36.4 million dollars (case 6 in Table 5). Because the users are at home after a day's work and before bed during the time frame (i.e., 17:00–21:00) and there is little solar energy that can be used, the daily electricity peak load concentrates on these periods. Thus it will need numerous solar PV to generate electrical energy and storage into big-sized batteries during the daytime to offset insufficient solar power at night.

It can be concluded that the WTs should be the main component in the hybrid system, and combined with moderately capacity of solar PV. Except the maximum TNPC case, the system without batteries has higher TNPC than that with batteries. Thus, a RE system combined with storage system is the optimal configuration from the TNPC perspective.

In the configurations of the grid-connected system, case 7 has the lowest TNPC of 9.0 million dollars, which obtained nearly 57% electricity less than that from the external grids completely (0.080 $/kW h of buying power). The system with big-sized solar PV and battery bank (5175 kW solar PV and 1200 batteries) has the maximum TNPC of 18.5 million dollars, indicating that too much capacity of solar PV is inappropriate in the residential community. This situation is similar to the stand-alone system. The system configurations that do have battery storage have lower TNPC, except the maximum TNPC scenario. This is because the excess renewable electricity can be stored and used at any follow-up time instead of importing from the external grids. Thus, the microgrid configuration with a small number of batteries would be cost-effective among all the grid-connected cases.

4. Conclusions

Maximizing the economic, technological and environmental benefits have become one of the major concerns for studies on microgrid systems. This paper investigates the feasibility of predominantly RE-based microgrids at an energy intensive power demand, then the techno-economic potential and optimal configuration are investigated under various RE-based stand-alone and grid-connected microgrid scenarios. HOMER power system simulation software is used with consideration of its public availability for microgrids modeling, and its ease of implementation. A residential community in Beijing is given to obtain the optimal configuration scheme for stand-alone and grid-connected microgrid systems, the technical and economic benefits of each optimized configuration are further evaluated.

The main conclusions of this paper can be summarized as follows: (1) there would be a very high potential for applying a predominantly RE-based microgrid in a residential community in Beijing, which could supply at least 90% of the onsite electricity demand with 47–100% renewable energy sources; (2) the TNPC of the grid-connected microgrid model would be at most 57% of the obtained electricity less than that completely from the external grids; (3) it would be more cost-effective when wind power becomes the main energy source and combined with moderately capacity of PV in the RE hybrid microgrid system; and (4) a system with moderate size of batteries would tend to be more ecologically friendly and cost-effective both in the stand-alone and grid-connected models than a system without batteries. These outputs can help decision makers determine the operation modes of the two types of microgrid systems: (1) DG power output characteristics; (2) system component composition optimization results; (3) systems component capacity optimization results; and (4) evaluation of the technical and economic benefits.

Two concerns are needed for further studies. Although this study considers RE sources such as wind energy and solar energy, other sources such as geothermal resources, biomass resources, and domestic waste that exist in cities could also be considered, and it is significantly desired to incorporate these resources into the optimal design of microgrid systems. Simultaneously, the triple supply of heat, electricity, and cold can make full use of local resources and realize the cascade utilization of energy. Moreover, this study uses HOMER software to build a microgrid system based on RE, with a single objective of minimizing the TNPC. Thus, a variety of software can be used for comparative analysis, and the commonalities and differences between different optimization results can be compared in the future research.

Acknowledgements

The authors thank the editor and the anonymous reviewers for their helpful comments and suggestions. This research was supported by the Strategic Priority Research Program of Chinese Academy of Sciences (XDA20040302) and Fundamental Research Funds for the Central Universities.

References

[1] He L, Chen YZ, Zhao HH, et al. Game-based analysis of energy-water nexus for identifying environmental impacts during Shale gas operations under stochastic input. Sci. Total Environ. 2018;627:1585–601.
[2] Chen Y, Lu H, Li J, et al. Regional planning of new-energy systems within multi-period and multi-option contexts: a case study of Fengtai, Beijing, China[J]. Renew Sustain Energy Rev 2016;65:356–72.
[3] Bayindir R, Hossain E, Kabalci E, et al. A comprehensive study on microgrid technology. Int J Renew Energy Res 2014;4(4):1094–107.
[4] Sreedharan P, Farbes J, Cutter E, et al. Microgrid and renewable generation integration 169 2016 University of California, San Diego. Appl Energy 2016;169:709–20.
[5] Dalton GJ, Lockington DA, Baldock TE. Feasibility analysis of stand-alone renewable energy supply options for a large hotel. Renew Energy 2008;33(7):1475–90.
[6] Mamaghani AH, Escandon SAA, Najafi B, et al. Techno-economic feasibility of photovoltaic, wind, diesel and hybrid electrification systems for off-grid rural electrification in Colombia. Renew Energy 2016;97:293–305.
[7] Mazzola S, Astolfi M, Macchi E. The potential role of solid biomass for rural electrification: a techno economic analysis for a hybrid microgrid in India. Appl Energy 2016;169:370–83.
[8] Xu Z, Nthontho M, Chowdhury S. Rural electrification implementation strategies through microgrid approach in South African context. Int J Electr Power Energy Syst 2016;82:452–65.
[9] Hafez O, Bhattacharya K. Optimal planning and design of a renewable energy based supply system for microgrids. Renew Energy 2012;45:7–15.
[10] Akinyele DO, Rayudu RK. Techno-economic and life cycle environmental performance analyses of a solar photovoltaic microgrid system for developing countries. Energy 2016;109:160–79.
[11] Bekele G, Palm B. Feasibility study for a standalone solar–wind-based hybrid energy system for application in Ethiopia. Appl Energy 2010;87(2):487–95.
[12] Goodbody C, Walsh E, McDonnell KP, et al. Regional integration of renewable energy systems in Ireland–the role of hybrid energy systems for small communities. Int J Electr Power Energy Syst 2013;44(1):713–20.
[13] Soshinskaya M, Crijns-Graus WHJ, van der Meer J, et al. Application of a microgrid with renewables for a water treatment plant. Appl Energy 2014;134:20–34.
[14] Chen YZ, He L, Li J. Stochastic dominant-subordinate-interactive scheduling optimization for interconnected microgrids with considering wind-photovoltaic-based distributed generations under uncertainty. Energy 2017;130:581–98.
[15] Alam M, Bhattacharyya S. Decentralized renewable hybrid mini-grids for sustainable electrification of the off-grid coastal areas of Bangladesh. Energies 2016;9(4):268.
[16] Chen Y, He L, Guan Y, et al. Life cycle assessment of greenhouse gas emissions and water-energy optimization for shale gas supply chain planning based on multi-level approach: case study in Barnett, Marcellus, Fayetteville, and Haynesville shales. Energy Convers Manag 2017;134:382–98.
[17] Bahramara S, Moghaddam MP, Haghifam MR. Optimal planning of hybrid

renewable energy systems using HOMER: a review. Renew Sustain Energy Rev 2016;62:609–20.
[18] Ramli MAM, Prasetyono E, Wicaksana RW, et al. On the investigation of photovoltaic output power reduction due to dust accumulation and weather conditions. Renew Energy 2016;99:836–44.
[19] Alzola JA, Vechiu I, Camblong H, et al. Microgrids project, Part 2: design of an electrification kit with high content of renewable energy sources in Senegal. Renew Energy 2009;34(10):2151–9.
[20] Gaona EE, Trujillo CL, Guacaneme JA. Rural microgrids and its potential application in Colombia. Renew Sustain Energy Rev 2015;51:125–37.
[21] Lambert T. PV Inputs. Homer Help File; 2007. Available from: 〈http://homerenergy.com/〉.
[22] T. Lambert How HOMER calculates the pv cell temperature homer help file 2007.[Available from]〈http://homerenergy.com/〉.
[23] T. Lambert How HOMER calculates the pv array power output homer help file 2007.[Available from]〈http://homerenergy.com/〉.
[24] Zhou W, Lou C, Li Z, et al. Current status of research on optimum sizing of stand-alone hybrid solar–wind power generation systems. Appl Energy 2010;87(2):380–9.
[25] Demoulias C. A new simple analytical method for calculating the optimum inverter size in grid-connected PV plants. Electr Power Syst Res 2010;80(10):1197–204.
[26] Sen R, Bhattacharyya SC. Off-grid electricity generation with renewable energy technologies in India: an application of HOMER. Renew Energy 2014;62:388–98.
[27] Kusiak A, Song Z. Design of wind farm layout for maximum wind energy capture. Renew Energy 2010;35(3):685–94.
[28] Goldwind Science & Technology [Internet]. Beijing: FreeMeso Mesoscale the Wind Resources Data Platform; c2015 [updated 2015; cited May 19].Chinese. Available from:〈http://freemeso.goldwind.com.cn/fjShop.aspx〉.
[29] T. Lambert How HOMER calculates wind turbine power output homer help file 2009.[Available from]〈http://homerenergy.com/〉.
[30] T. Lambert Wind resource inputs homer help file 2009.[Available from]〈http://homerenergy.com/〉.
[31] Ozoemena M, Hasan R, Cheung WM. Analysis of technology improvement opportunities for a 1.5 MW wind turbine using a hybrid stochastic approach in life cycle assessment. Renew Energy 2016;93:369–82.
[32] Wang C, Liu Y, Li X, et al. Energy management system for stand-alone diesel-wind-biomass microgrid with energy storage system. Energy 2016;97:90–104.
[33] Hemmati R, Saboori H. Emergence of hybrid energy storage systems in renewable energy and transport applications–A review. Renew Sustain Energy Rev 2016;65:11–23.
[34] Saheb-Koussa D, Koussa M, Haddadi M, et al. Hybrid options analysis for power systems for rural electrification in Algeria. Energy Procedia 2011;6:750–8.
[35] T. Lambert Battery details window homer help file 2004.[Available from]〈http://homerenergy.com/〉.
[36] T. Lambert Generator minimum load homer help file 2004.[Available from]〈http://homerenergy.com/〉.
[37] Li J, He L, Lu H, et al. Stochastic goal programming based groundwater remediation management under human-health-risk uncertainty. J Hazard Mater 2014;279:257–67.
[38] Chauhan A, Saini RP. Techno-economic feasibility study on integrated renewable energy system for an isolated community of India. Renew Sustain Energy Rev 2016;59:388–405.
[39] T. Lambert Total net present cost homer help file 2009.[Available from]〈http://homerenergy.com/〉.
[40] Liu G, Rasul MG, Amanullah MTO, et al. Techno-economic simulation and optimization of residential grid-connected PV system for the Queensland climate. Renew Energy 2012;45:146–55.
[41] Shirazi A, Taylor RA, White SD, et al. Transient simulation and parametric study of solar-assisted heating and cooling absorption systems: an energetic, economic and environmental (3E) assessment. Renew Energy 2016;86:955–71.
[42] Bilal BO, Sambou V, Kébé CMF, et al. Methodology to size an optimal stand-alone pv/wind/diesel/battery system minimizing the levelized cost of energy and the CO_2 emissions. Energy Procedia 2012;14:1636–47.
[43] Montuori L, Alcázar-Ortega M, Álvarez-Bel C, et al. Integration of renewable energy in microgrids coordinated with demand response resources: economic evaluation of a biomass gasification plant by Homer Simulator. Appl Energy 2014;132:15–22.
[44] Sundaramoorthy K. Development of the hard and soft constraints based optimisation model for unit sizing of the hybrid renewable energy system designed for microgrid applications. Int J Sustain Energy 2017;36(2):192–208.
[45] Rawat R, Chandel SS. Simulation and optimization of solar photovoltaic-wind stand-alone hybrid system in hilly terrain of India. Int J Renew Energy Res (IJRER) 2013;3(3):595–604.
[46] Sivarasu SR, Sekaran EC, Karthik P. Development of renewable energy based microgrid project implementations for residential consumers in India: scope, challenges and possibilities. Renew Sustain Energy Rev 2015;50:256–69.
[47] Abdilahi AM, Yatim AHM, Mustafa MW, et al. Feasibility study of renewable energy-based microgrid system in Somaliland′ s urban centers. Renew Sustain Energy Rev 2014;40:1048–59.
[48] HOMER Energy Knowledgebase [Internet] Dec - [cited 2016 Jul 7]; 2010. Available from: 〈http://support.homerenergy.com/index.php?/Knowledgebase/Article/View/264/0/10059—cycle-charging—specifying-a-setpoint-soc〉.
[49] Chen YZ, He L, Zhao HH, et al. Energy-environmental implications of shale gas extraction with considering a stochastic decentralized structure. Fuel 2018;230:226–43.